Dalton Transactions

An international journal of inorganic chemistry

Accepted Manuscript

This article can be cited before page numbers have been issued, to do this please use: K. C. Kamashanju, M. Curtil, F. Molton, N. Vlachopoulos, F. Thomas and J. Chauvin, *Dalton Trans.*, 2026, DOI: 10.1039/D6DT00748A.

ROYAL SOCIETY OF CHEMISTRY

rsc.li/dalton

Synthesis, characterisation and properties towards CO_2 reduction into CO of a Cr(III) diphenyl quaterpyridine complex.

View Article Online
DOI: 10.1039/D6DT00748A

Kabibi-Charles Kamashanju, Mathieu Curtil, Florian Molton, Nikolaos Vlachopoulos, Fabrice Thomas, Jérôme Chauvin*

Univ. Grenoble Alpes, CNRS, DCM UMR 5250, F-38000 Grenoble, France, E-mail: jerome.chauvin@univ-grenoble-alpes.fr

Abstract:

During the last decade, group VI metals have regained interest in synthesizing inorganic complexes that demonstrate catalytic properties for CO_2 reduction. However, these complexes often exhibit high overpotential and poor efficiency compared to those constructed with less-abundant metals. In this work, a polypyridinyl complex consisting of a Cr(III) centre coordinated to the tetradentate 4',4"-diphenyl-2,2':6',2":6",2"'-quaterpyridine ligand and two monodentate chloride ligands ($[Cr(dpqpy)Cl_2]^+$) has been synthesized and characterized. Cyclic voltammetry performed under argon displays three quasi-reversible one-electron systems in the cathodic part. Zn(II) parent complex ($[Zn(dpqpy)Cl_2]$) was also synthesized and investigated to identify the nature of the reduction events. The three reduced species of $[Cr(dpqpy)Cl_2]^+$ were generated by exhaustive electrolysis and characterized by ultraviolet-visible and electron paramagnetic resonance spectroscopies. Density functional theory calculations confirmed that the two last reduction are localized on the quaterpyridine ligand. Under CO_2 with $[Cr(dpqpy)Cl_2]^+$ dissolved in DMF in the presence of phenol, a catalytic current is observed during the last reduction at an onset potential of -1.72 V *vs* $Ag/AgNO_3$ (10^{-2} M). Exhaustive electrolysis of $[Cr(dpqpy)Cl_2]^+$ performed at -1.85 V under CO_2 in DMF + 0.1 M $TBAPF_6$ in presence of 1.25 M of phenol led to the formation of CO with a faradaic efficiency of 60% after 2hrs, with no H_2 being detected during the reaction time. Longer experiments lead to a partial degradation of the complex.

View Article Online
DOI: 10.1039/D6DT00748A

Introduction:

With a continuous increase in the consumption of fossil fuels as a result of anthropogenic activities, the emission of greenhouse gases such as carbon dioxide has led to a considerable climatic change. It now becomes crucial to diminish its concentration in the atmosphere. One answer of the problem can be the transformation of the molecule after its capture. CO_2 being inert and the most oxidized form of carbon, its conversion requires then an electron source for reduction as well as selective catalysts.[1] Indeed depending on the number of electrons and protons involved in the process, the CO_2 reduction reaction (CO_2RR) leads to several products such as CO, HCOOH, H_2CO, CH_3OH, CH_4, whereas the competitive reduction of protons occurs in the same potential range.[2] If the chemicals provided by CO_2 reduction is beneficial for the foreseeable future, this transformation stays a challenging process. [3] Notably it requires a large Gibbs free energy input of around 300 kJ/mol which makes the reaction cumbersome. To circumvent this large energy barrier, a catalyst is necessary to open up routes for less energy-demanding reactions by stabilizing the intermediate transition states between the linear CO_2 molecules and the intended product.[4] Among different molecular catalyst, polypyridyl complexes built with a noble metal centre such as Re(I), Ru(II), or Rh(III) have proven their efficiency in the 2e- catalytic reduction of CO_2 since the 1980's.[5-7] Alternatives constructed with 1st raw metal centre such as Mn(I), Ni(II), Co(III) or Fe(II) have also shown interesting behavior and various examples are reviewed in litterature.[8-11] Polypyridyl complexes of Cr are however still underexplored despite the large accessibility of this metal on Earth.[12,13] $[Cr(bpy)(CO)_4]$ (bpy = 2,2' bipyridine) was notably investigated by F. Hartl and co-workers, and showed moderate catalytic activity and quite high overpotential. The pentacoordinate species $[Cr(bpy)(CO)_3]^{2-}$ formed upon two-electron reduction is hinted to be the active catalytic species for CO_2RR.[14] In the mid-90s, Abruña and co-workers reported a Cr(III) complex designed with a bis-4'-vinylterpyridine ligand which upon electropolymerization onto a glassy carbon electrode exhibited an electrocatalytic activity under CO_2 towards the formation of formaldehyde (H_2CO) as a predominant reduction product. The formation of H_2CO was attributed to a cooperative effect between two or more metal centres in the electrodeposited film.[15] More recently, Machan and co-workers proposed a series of Cr(III) complex built with a tetradentate ligand which consists of a 2,2'-bipyridine with two phenolate moieties or a terpyridine core with a phenolate substituant.[16,17] These complexes are capable of selectively reducing CO_2 into CO, with phenol as a proton source, in acetonitrile. Following this approach J. W. Wang et al. have studied a quaterpyridinyl (qpy) complex of Cr(III) for CO_2 reduction. They reported an almost 100% faradaic efficiency for CO production in DMF/phenol mixture

View Article Online
DOI: 10.1039/D6DT00748A

with a turn over frequency of 86.6 s^{-1} these values are obtained at -2 V vs Fc^+/Fc after 30 min of electrolysis.[18] Quaterpyridine-based ligands were already used to prepare other complexes with a first -row metal centre such as Co(II)[19], Cu(II)[20] or Fe(II)[21] showing good activity towards the catalysis of CO_2 reduction. Indeed, as good π-acceptor ligands, resistant to oxidation, qpy leads to the formation of stable metal complexes in high oxidation state, and favour CO_2 reduction at relatively low potential values.[22]

In such a context, we decided to synthesize a modified structure $[Cr^{III}(dpqpy)Cl_2]^+$ (dpqpy = 4',4''- diphenyl-2,2':6',2'':6'',2'''-quaterpyridine), (scheme 1) and investigate its electrochemical properties in the context of the CO2RR. The dpqpy ligand offers higher aromaticity than qpy, which could improve the electron storage capacity of the complex under reducing conditions. The synthesis of the ligand and the corresponding $[Cr^{III}(dpqpy)(Cl)_2]Cl$ complex was carried out following the publications of Constable et al.[23,24] The related zinc complex $[Zn^{II}(dpqpy)(Cl)_2]$ was also synthetized to study the electrochemical behaviour of the ligand with a redox inactive metal centre. The electrocatalytic properties of $[Cr^{III}(dpqpy)(Cl)_2]^+$ complex in the dissolved state regarding the CO_2 reduction into CO are the focus of the present research. Spectroelectrochemistry and electron paramagnetic resonance (EPR) spectroscopy, both coupled with density functional theory (DFT) calculations, were also performed in order to characterise the different reduction states of this complex. Under CO_2, the production of CO is confirmed and followed by GC-MS experiments under exhaustive electrolysis during 3h to study the robustness of the complex.

Experimental section:

Materials and compounds. All the starting materials and solvents for synthesis were obtained from commercial sources without further purification. $CrCl_3.6H_2O$ (98%), $ZnCl_2$ (98%) and tetrabutylammonium hexafluorophosphate ($TBAPF_6$) were purchased from Sigma Aldrich. A 3 mm diameter (0.071 cm^2 area) glassy carbon disk electrode was used in all cyclic voltammetry (CV) and rotating disk electrode (RDE) experiments. For bulk electrolysis, a porous carbon foam electrode (Duocel ERG aerospace, 80 dpi) was used.

Instrumentation. *Ultraviolet-visible (UV-VIS) and infrared (IR) spectroscopies*. UV-VIS spectra of complexes in solution were recorded on a Cary 50 Probe UV− VIS spectrophotometer (VARIAN) or on a Zeiss MC5601 spectrophotometer, using either a 1 mm quartz immersion probe (Hellma Inc.) or a quartz cuvette of optical path length l =1 cm. IR spectra were recorded

View Article Online
DOI: 10.1039/D6DT00748A

using a "Golden Gate" ATR system. This system features a brazed diamond ATR crystal and a signature "Golden Gate" sample loading bridge. The complex samples in solid form were loaded on this bridge which contains the required mirrors for beam transmission.

Electrochemistry. Cyclic voltammetry scans were performed on a Model SP-300 potentiostat (BioLogic) in a standard three electrodes cell (glassy carbon working electrode; $Ag/AgNO_3$ 10^{-2} M in DMF + 0.1 M $TBAPF_6$ as reference electrode; platinum as auxiliary electrode) (**Figure S1**). Using this reference electrode, the potentials can be converted to Fc^+/Fc by subtracting 87 mV or SHE by adding 542 mV.[25] Experiments under argon were performed in a glovebox (Jacomex).

Electrocatalysis. Experiments were carried out at room temperature in a CO_2 saturated environment in a sealed conventional three-electrode cell. The reference and counter electrodes were $Ag/AgNO_3$ 0.01 M and Pt plate, respectively, carbon foam (Duocel ERG aerospace, 80 dpi) was used as working electrode material. In a normal setting with 3 electrodes and 10 mL solution, the headspace volume was measured to be 140 mL (**Figure S1**). During the experiments, at each time interval a 100 µL sample was taken from the headspace gas using a gas-tight injection syringe. Gas products were analyzed on a Perkin Elmer Clarus 590 gas chromatography (GC) instrument equipped with two columns, a Restek Hayesep Q (L = 2 m, diam. = 1 mm), a Restek molecular sieve 5A (L = 2 m, diam. = 1 mm), and using argon as vector gas. In GC, thermal conductivity and flame ionisation detection (TCD, FID) were used for H_2 (TCD), CO (FID) CH_4 (FID). The limits of quantification are estimated to 80 ppm for H_2, 30 ppm for CO and CH_4. Calibration was performed with a gas mixture standard $H_2/CO/CH_4$ 1% each in CO_2. At the end of the experiments, the solution was analysed by manual injection of 20 µL on a Metrohm Eco ionic chromatograph equipped with a Metrosep A supp 19 column in which Na_2CO_3 8mM / $NaHCO_3$ 0.25 mM in water was used as mobile phase for formate detection by conductivity. The uncertainties of the faradaic efficiency were estimated by comparison of the results of two similar experiments.

Mass Spectroscopy. High Resolution Mass Spectrometry (HRMS) spectra were recorded on an LTQ orbitrap XL thermo scientific instrument in electrospray ionisation (ESI) positive mode.

EPR spectroscopy. X- and Q- band EPR spectra were recorded with a Bruker EMX instrument, equipped with the ER-4192 ST Bruker and ER-4121 VT for the X-band at 100 K experiments and the ER5106 QTW Bruker cavity and an Oxford Instruments ESR-900 continuous-flow helium cryostat for the Q-band at 4.5 K experiments.

View Article Online
DOI: 10.1039/D6DT00748A

DFT calculation. Full geometry optimizations were performed with the Gaussian 9 program,[26] by using the B3LYP exchange-correlation functional.[27,28] Dispersion was taken in account by using the Grimme D3 correction.[29] Two basis sets were investigated for the Cr, C, H, N atoms: the double zeta 6-31g*,[30] as well as the triple zeta 6-311+G(2d,p).[31,32] Frequency calculations were systematically performed in order to ensure that the optimized structure corresponds to a minimum and not to a saddle point. The solvent (DMF) was considered by using a polarized continuum model.[33] The energies discussed in the text correspond to the sum of electronic and thermal free energies, expressed in kcal/mol, at 298 K.

Synthesis. [Cr(dpqpy)(Cl)$_2$]Cl. 0.13 mmol (0.027 g) of $CrCl_3.6H_2O$ was mixed with 0.1 mmol (0.046 g) of 4',4''-diphenyl-2,2':6',2'':6'',2'''-quaterpyridine in 15 mL of ethanol, this solution was refluxed for 30 h under N_2. After cooling, the solution was filtered resulting to a greenish-grey solid product that was then rinsed with ethanol and dried using diethyl ether. Yield: 62% (38.8 mg). FT-IR: 1603s, 1545s, 1487w, 1461s, 1407s, 1242s, 1049w, 1024s, 886w, 830w, 787w, 769s, 731s, 689s cm^{-1}. HRMS: m/z $[M]^+$ = 582.06754 (calculated for $C_{32}H_{22}N_4Cl_2Cr$: 582.06765). Elem. Anal. calculated for $C_{32}H_{22}N_4Cl_3Cr$, $3H_2O$: C: 56,95 %; H: 4,18 %; N: 8,30 % found: C: 56,64 %; H: 3,91%; N: 8,29 %.

[Zn(dpqpy)(Cl)$_2$]. 7.5×10^{-2} mmol (0.010 g) of $ZnCl_2$ was mixed with 5.2×10^{-2} mmol (0.024 g) of 4',4''-diphenyl-2,2':6',2'':6'',2'''-quaterpyridine in 20 mL of ethanol, the solution was refluxed for 2 h under Ar. After cooling, the solution was filtered and evaporated, resulting to a white solid product (12.0 mg)**.** FT-IR: 1602vs, 1555s, 1486w, 1459s, 1402s, 1247s, 1162w, 1015s, 891w, 795w, 764s, 733w, 682w cm^{-1}. HRMS: m/z $[M\text{-}2Cl]^{2+}$ = 263.0561 (calculated for $C_{32}H_{22}N_4Zn$: 263.05625).

Results and discussion:

Synthesis and photophysical characterisation of [Cr(dpqpy)(Cl)$_2$]$^+$.

Chromium [4',4''-diphenyl-2,2':6',2'':6'',2'''-quaterpyridine] bis-chloro complex, with chloride as counter anion ([Cr(dpqpy)(Cl)$_2$]Cl), was synthesized using hydrated chromium (III) chloride salt and diphenyl quaterpyridine (dpqpy) as starting materials, as depicted in **Scheme 1**, following an adapted procedure from literature.[23] Given the inert nature of the Cr^{3+}, the complexation procedure was found to be kinetically slow. After a reflux reaction in ethanol for 30 hours under nitrogen, a grey solid powder was collected by filtration. The synthesis is confirmed by HRMS, showing a mass peak and isotopic pattern in accordance with the expected formula (**Figures S2, S3**).

View Article Online
DOI: 10.1039/D6DT00748A

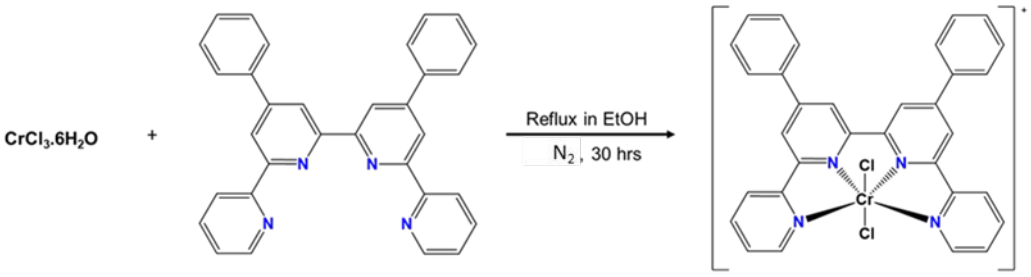

Scheme 1. Synthesis procedure for $[Cr(dpqpy)(Cl)_2]^+$ complex.

The complex is sparingly soluble in CH_3CN, THF or CH_2Cl_2 and more soluble in DMF, providing a faint brown-gold solution. UV-VIS spectrum displayed a strong absorption band in the UV region corresponding to the ligand-centred allowed $\pi \rightarrow \pi^*$ transition ($\lambda_{max.}$ = 323 nm, ε = 4×10^4 $M^{-1}cm^{-1}$). Additionally, a weak absorption in the visible is detected with a maximum located around 540 nm (ε = 250 $M^{-1}cm^{-1}$). This band is associated to the forbidden metal-centred transitions (**Figure 1**).

The Zn(II) analogue complex was also synthesized in order to further elucidate the electrochemical properties of the Cr complex (see further in the text). The complexation occurs in two hours starting with $ZnCl_2$ and dpqpy in ethanol. The solution remains colourless in the course of the reaction as Zn(II) has a d^{10} configuration.

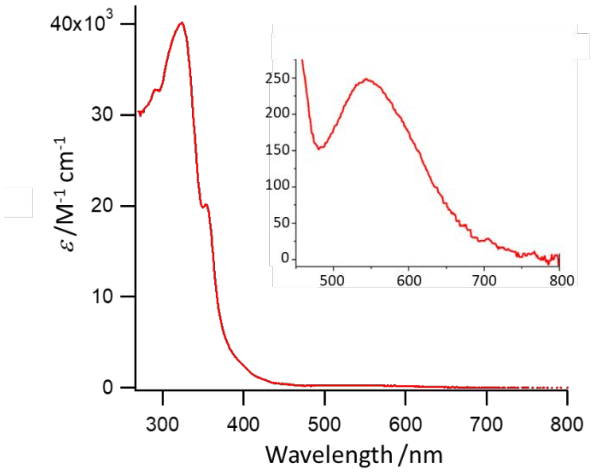

Figure 1 Electronic absorption spectrum of $[Cr(qpy)(Cl)_2]^+$ in DMF; inset zoom in the visible region. ε : molar extinction coefficient.

Electrochemistry under argon.

View Article Online
DOI: 10.1039/D6DT00748A

All the compounds were characterized by cyclic voltammetry (CV) in an argon-saturated DMF solution with 0.1 M $TBAPF_6$ as supporting electrolyte. Whereas the CV of the free ligand (dpqpy) shows in the cathodic part two chemically irreversible reduction waves at a cathodic peak potential of Epc = - 2.36 V and - 2.69 V *vs* $Ag/AgNO_3$ (**Figure S4**), $[Zn(dpqpy)(Cl)_2]$, exhibits two quasi-reversible monoelectronic systems at $E_{1/2}$ (V) = -1.56V (with a peak separation of ΔEp = 75mV); -1.82V (ΔEp = 130mV) (**Figure S5)**. As Zn(II) is redox inert, the 2 reduction events are centred on the ligand. $[Cr(dpqpy)(Cl)_2]Cl$ shows in the same potential range a series of three quasi-reversible systems at $E_{1/2}$ (V) = -1.03V (ΔEp =70mV) ; -1.48V (ΔEp =110mV); -1.79V (ΔEp =70mV) (**Figure 2).** The two last ones appear at a close potential than the reduction systems of $[Zn(dpqpy)(Cl)_2]$ and could then be attributed to the stepwise reduction of the ligand, whereas the first reduction event at $E_{1/2}$ (V) = - 1.03V does not appear in $[Zn(dpqpy)(Cl)_2]$ and may be attributed to the reduction of the Cr(III) center into a Cr(II) one. EPR and DFT calculations were performed to confirm the attribution (see further in the text).

In the anodic part $[Cr(dpqpy)(Cl)_2]Cl$ exhibits a chemically irreversible system at an anodic peak potential of Ep_a = 0.58V attributed to the oxidation of the chloride counter anion in solution.[34] Indeed a related Cr(III) polypyridine complex such as $[Cr(ttpy)_2](ClO_4)_3$ (ttpy = 4'-(4-methylphenyl)-2,2':6,2''-terpyridine) does not exhibit any oxidation wave in this potential range,[35] whereas tetraethylammonium chloride $[N(Et)_4]^+,Cl^-$ salt in DMF shows an irreversible oxidation wave at 0.58V (**Figure S6**). Rotating disk electrode (RDE) experiments show that this oxidation requires the same number of electron than the first reduction step of the complex (**Figure S7**). It indicates that the two chloro ligands are not exchanged with solvent molecules. Exhaustive bulk electrolysis performed at Ep_a = 0.6 V consumed one electron per complex. The CV recorded after this exhaustive electrolysis is similar to the initial CV of the complex in the cathodic part, showing the three one-electron reduction events at similar potential values (**Figure S8**). This behaviour is in accordance with the oxidation of the counter anion.

View Article Online
DOI: 10.1039/D6DT00748A

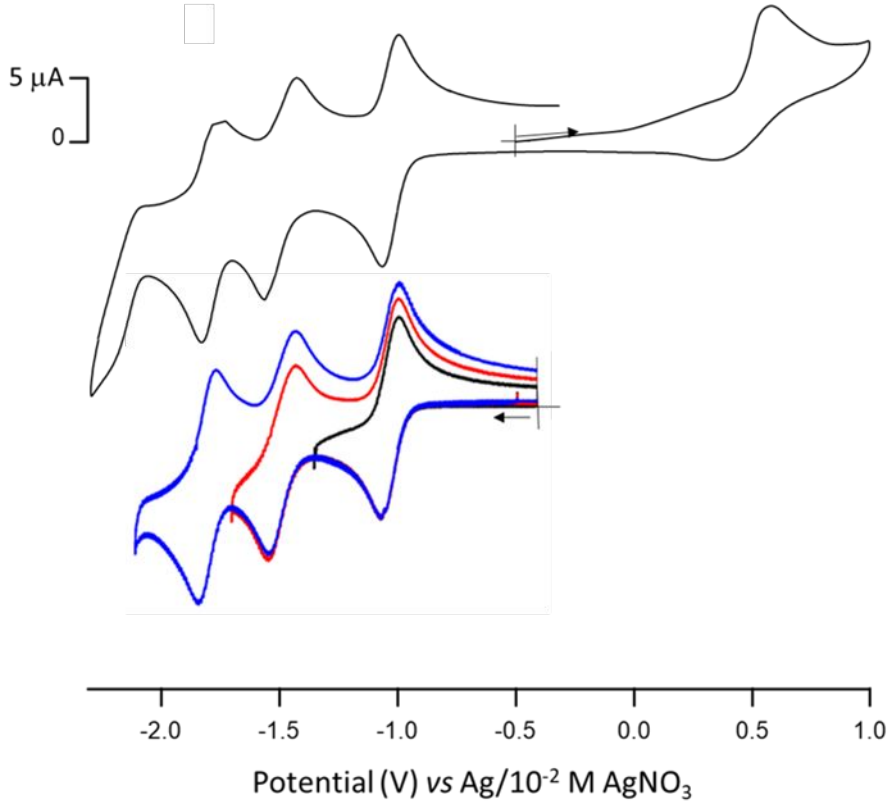

Figure 2 Cyclic voltammetry scan of 1mM $[Cr(dpqpy)(Cl)_2]Cl$ in DMF/0.1M $TBAPF_6$ under argon atmosphere on a GCE at a scan rate of $0.1Vs^{-1}$: above in the anodic direction, below in the cathodic direction showing three different reduction waves recorded between -0.5V to -1.43 V; -0.5 V to -1.78 V and -0.5V to -2.18V. Electrode surface 0.071 cm^2

CV measurements recorded in reduction at different scan rates show, a correlation between the square root of scan rate and the peak current intensity i_p (**Figure S9)**. The linear trend of the Randles–Ševčík plot is common in all of the three redox processes and indicates that these three redox waves are diffusion-controlled processes, proving that the complex does not stick at the surface of the GC electrode. Using the Randles–Ševčík equation at 20°C (eq.1), the diffusion coefficient of $[Cr(dpqpy)(Cl)_2]^+$ is estimated to 2.82×10^{-6} cm^2/s

$$I_p = 2.69 \times 10^5 \times A \times D^{1/2} \times C \times v^{1/2} \qquad \text{(eq.1)}$$

In this equation, A is the surface of the electrode in cm^2, C the concentration in mol/cm^3 and v the scan rate in Vs^{-1}.

View Article Online
DOI: 10.1039/D6DT00748A

To investigate the stability of the different reduction state of the complex in solution, exhaustive bulk electrolysis was performed at each reduction potential of $[Cr(dpqpy)(Cl)_2]^+$. **Figure 3** shows the CV and RDE experiments obtained after electrolysis. RDE shows that the redox processes have a similar current magnitude prior and after the two first electrolysis experiments performed at -1.07 and -1.55 V. After the third electrolysis performed at -1.83 V, the signal exhibits a lower intensity compared to others due to a lower solubility of the fully reduced species. The CV scan recorded after each reduction are depicted in **Figure 3B**. After the first electrolysis experiment at -1,07V, the CV of the solution presents two redox waves at a similar position than that of the initial solution. It proves the full reversibility of the first electron transfer process. However, after the reduction performed at -1.55 V, the CV scan shows the emergence of two new waves, each marked by an asterisk, indicating that the complex undergoes a slow chemical transformation under such a reductive condition.

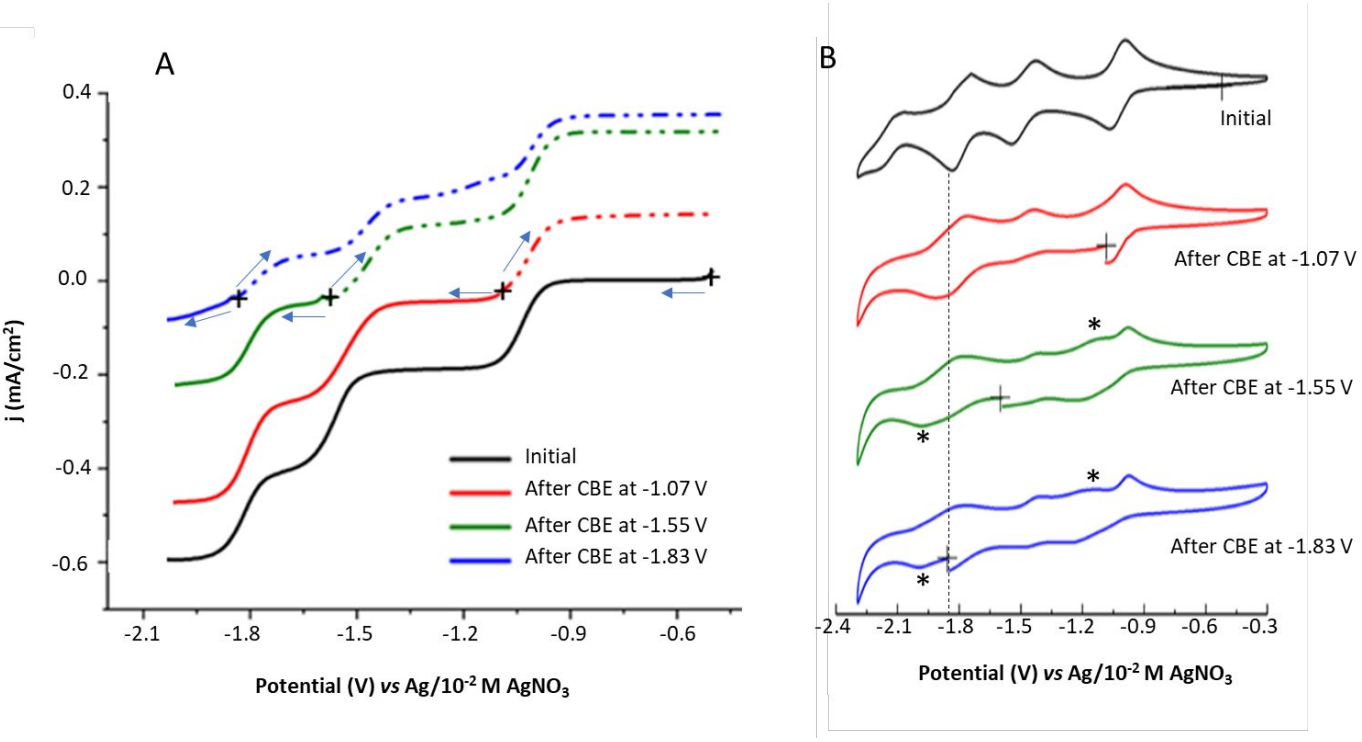

Figure 3 A: Cathodic (solid lines) and anodic (dash-dot lines) cyclic voltammetry scans prior and after electrolysis of 1mM $[Cr(dpqpy)(Cl)_2]^+$ complex under argon on a rotating disk electrode (rate of rotation : 200 rpm, scan rate : 10 mV s^{-1}, electrode area : 0.071 cm^2); **B**: cathodic CV scans after electrolysis of 1mM $[Cr(dpqpy)(Cl)_2]^+$ complex under argon on a glassy carbon electrode in DMF/0.1M $TBAPF_6$ at a scan rate of 0.1Vs^{-1}, electrode area 0.071 cm^2

To characterize the nature of the transformation, CV experiments were performed on a wider potential window, including the anodic part (**Figure S10**). Prior to electrolysis, the CV scan shows the oxidation peak at 0.58 V, attributed to the oxidation of the chloride counter ion in

View Article Online
DOI: 10.1039/D6DT00748A

solution. After the first electrolysis process, at -1.07 V, the current magnitude corresponding to the chloride oxidation process was not modified; however, upon electrolysis at the second reduction peak (-1.55 V), the increase of current density suggests an accumulation of released chloride ions in solution (**Figure S10**). This should account from the discoordination of the Cl^- linked to the metal centre. This oxidation process that emerges after the second reductive electrolysis was deduced to be a 2-electron oxidation process per complex by RDE voltametry (**Figure S10B)**. It is then attributed to one Cl^- counter ion and one coordinated Cl^- ion released in solution after electrolysis at -1.55V. The bis-reduced complex is then assumed to undergo a transformation, associated to the release of one chloride ion resulting into the formation of $[Cr^{III}(dpqpy^{2-})(Cl)(DMF)]$**.** This new species can account for the appearance of a new reduction peak (≈ -1.95V) in the cathodic CV scan (**Figure 3B**).

Electronic absorption spectra were recorded after the 3 successive exhaustive electrolysis steps of $[Cr(qpy)(Cl)_2]^+$ performed in DMF, in order to characterize the different redox states of the complex. Prior to electrolysis, one strong absorption band in the UV region and a weak absorption band at 540 nm are observed as discussed previously. (**Figure 4**)

View Article Online
DOI: 10.1039/D6DT00748A

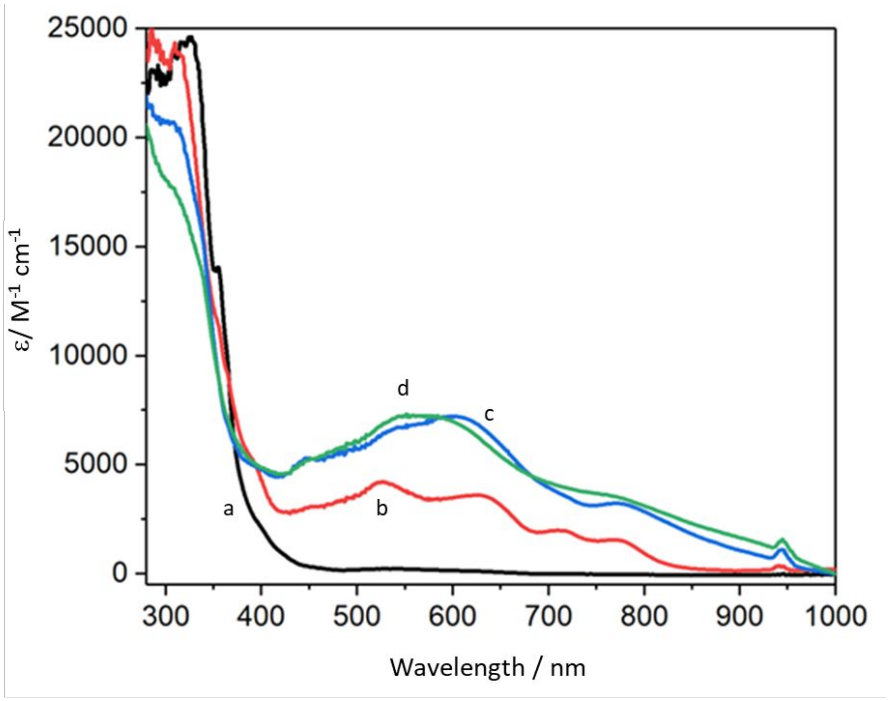

Figure 4 Ultraviolet-visible-near infrared absorption spectra of 1mM $[Cr(qpy)(Cl)_2]^+$ in DMF/0.1 M $TBAPF_6$: (a) initial solution, (b) after exhaustive electrolysis at −1.03 V, (c) after exhaustive electrolysis at −1.49 V, and (d) after exhaustive electrolysis at −1.79 V. ε : molar extinction coefficient.

The mono-reduced $[Cr(qpy)(Cl)_2]$ species exhibits in the visible range two absorption bands at 528 nm (ε = 4 200 $M^{-1}cm^{-1}$) and 628 nm (ε = 3 500 $M^{-1}cm^{-1}$), plus two other weak shoulder peaks around 713 nm (ε = 2 100 $M^{-1}cm^{-1}$) and 773 nm (ε = 1 700 $M^{-1}cm^{-1}$). Further electrolysis at -1.55 V led to the formation of a ligand reduced species whose absorption bands extend to the whole visible part of the spectrum reaching a maximum at 601 nm (ε = 8 000 $M^{-1}cm^{-1}$). In course of electrolysis at -1.55V, the solution colour changed from faint golden-brown to deep purple. The final tris-reduced species is less soluble, and might decomposed. The solution exhibits an absorption maxima at around 568 nm as shown in **Figure 4**.

EPR characterisation and DFT calculations.

Electron paramagnetic resonance (EPR) spectroscopy was performed to confirm the assignation of the adding electron upon successive reduction of $[Cr^{III}(dpqpy)(Cl)_2]^+$. **Figure 5** presents EPR

View Article Online
DOI: 10.1039/D6DT00748A

spectra recorded at the X-band frequency (ν ≈ 9.65GHz) at 20 K prior to and after successive bulk reductive electrolysis steps.

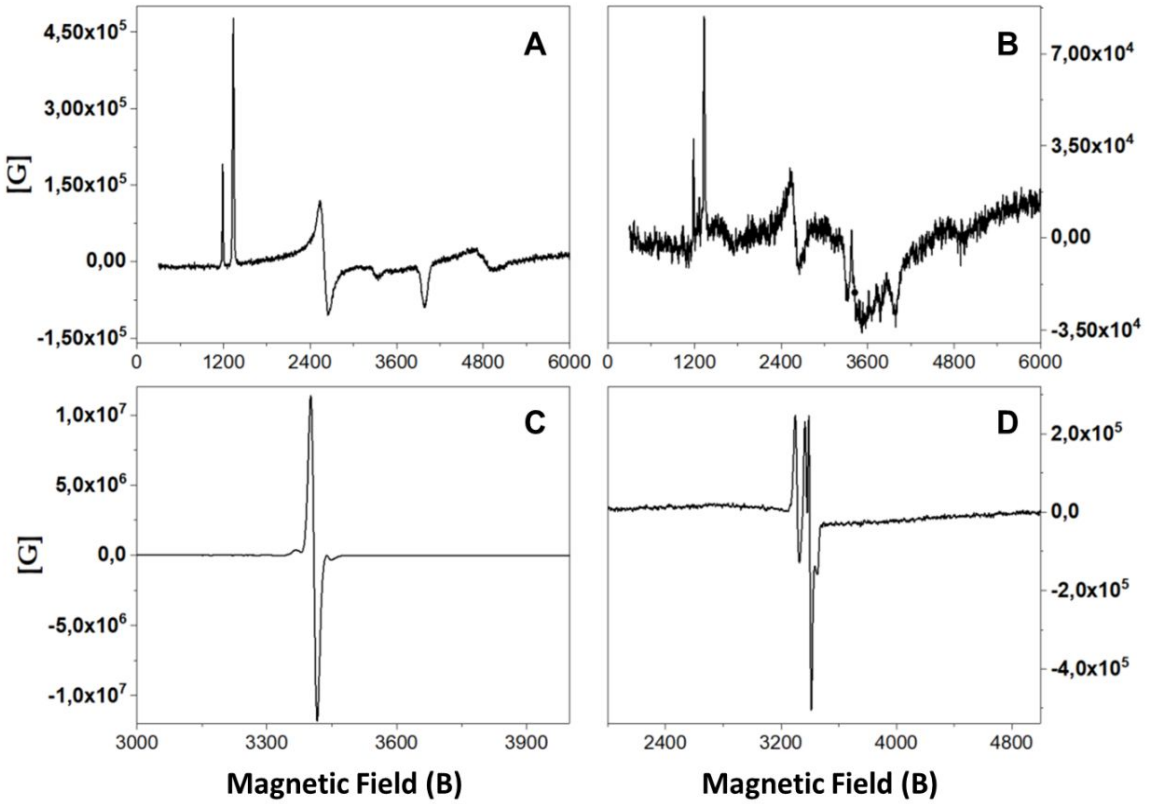

Figure 5. Electron paramagnetic resonance spectra of 1mM $[Cr^{III}(dpqpy)(Cl)_2]^+$ in DMF/0.1M $TBAPF_6$ prior (A) and after electrolysis at -1.07 V (B) at -1.55 V (C) at -1.83 V (D).

The EPR spectrum of $[Cr^{III}(dpqpy)(Cl)_2]^+$ (**Figure 5A**) covers a large spectral window, with resonances at g = 5.7, 5, 2.6, 1.7 and 1.4. It is typical of a high spin (S =3/2) Cr^{III} complex.[36] By taking into consideration a one-electron reduction, the putative spin states are S = 2, 1 or 0. The spectrum depicted in **Figure 5B** shows that the species generated upon one-electron reduction is X-band EPR silent. A ground spin state ($S = 0$) is very unlikely, given the geometry, thus we propose that the one-electron reduced species is an integer spin system, but the zero field splitting parameters are too large to allow for its detection at the X-band frequency.

Accordingly, the two-electron reduction of $[Cr^{III}(dpqpy)(Cl)_2]^+$ results in the growing of a strong signal at g = 1.98, which is reminiscent of an (S = 1/2) spin state (**Figure 5C**). The g value is close to 2, indicative of a significant radical character on the complex. Finally, the three-electron reduction is accompanied by a quenching of the S = 1/2 resonance, concomitant

View Article Online
DOI: 10.1039/D6DT00748A

with the appearance of minor resonances attributed to unidentified decomposition products (**Figure 5D**).

DFT calculations

To gain insights into the electronic structures of the electron-transferred series, we performed density functional theory (DFT) calculations, using the B3LYP hybrid functional. Full computational details, including Cartesian coordinates, energetic analyses, and selected Mulliken spin population data (B3LYP, D3-B3LYP, D3-B3LYP/PCM and D3-B3LYP/PCM with a triple zeta basis set), are provided in the ESI, (**Figures S11-S29** and **Tables S1-S6)**. **Table 1** summarizes the most stable electronic structures of the complex in its different reduction states. The trends in the energy ranking for all spin states considered, as well as their formulation, were similar when using the B3LYP, D3-B3LYP, and D3-B3LYP/PCM functionals (with double zeta 6-31 g* basis set), as well as D3-B3LYP/PCM with a split valence triple zeta basis set (6-311+G(2d,p) (**Table S2**). For clarity, only results obtained using the D3-B3LYP/PCM/6-31g* approach are presented here, unless otherwise stated. Since the three-electron reduced species was found to decompose during electrolysis, it was not included in the calculations.

Geometry optimization of quartet $[Cr(dpqpy)(Cl)_2]^+$ yielded an octahedral metal ion (**Figure 6a**). A comparison of structural parameters within the coordination sphere of the related complex based on unsubstituted quaterpyridine revealed a very good agreement between experiment and theory.[18] The two distinct Cr-N and the Cr-Cl bond distances were indeed reproduced with deviations that do not exceed 0.01, 0.03, and 0.06 Å, respectively. Furthermore, frequency and TD-DFT calculations accurately predict the experimental IR and absorption spectra, validating our methodology (**Figure S22** and **S27**). The Mulliken spin population analysis revealed a value of 3.07 on the Cr atom, confirming that the spin density is predominantly localized on a Cr(III) centre. This value will be taken as a reference for assigning the metal's formal oxidation state in the electron-transferred series.

For the octahedral one-electron reduced species $[Cr(dpqpy)(Cl)_2]$, both triplet (S=1) and quintet (S=2) spin states were considered (**Table S2**), and calculation predicts the first to be the ground spin state. The calculated Mulliken spin populations on the metal centre are 2.97 and 3.08 for the triplet and quintet, respectively. The second value is very close to that computed for $[Cr(dpqpy)(Cl)_2]^+$, indicative of a Cr(III) metal ion, while the first is slightly lower, consistent

View Article Online
DOI: 10.1039/D6DT00748A

with the lower spin state. Thus, both states mostly correspond to octahedral Cr(III)-ligand radical systems, denoted as [Cr(dpqpy•⁻)(Cl)$_2$]. Notably, the ligand radical's spin density is primarily localized on the central bipyridine subunit in a symmetric manner, with negligible delocalization onto the phenyl rings. The broken-symmetry (3,1) nature of the triplet state was further confirmed by a negative Mulliken spin population on the ligand and a positive value on the Cr atom, where the quintet exhibits positive values only (**Figure 6b,c**). This conclusion matches that reached by Wieghardt *et al.* on one-electron reduced octahedral Cr(III) bis(terpyridine) complexes [37] but contrasts with that recently reported for a related one-electron reduced quaterpyridine Cr(III) complex (metal-centred reduction), lacking axial ligands. While no electrochemical evidence for ligand dissociation upon one-electron reduction was found in the present series, we nonetheless reoptimized a structure in which the metal centre is formally uncoordinated in the axial positions ([Cr(dpqpy)]$^{2+}$). Under these conditions, the calculations converged towards a quintet square-planar Cr(II) species (**Table S2**). This highlights the strong sensitivity of the electronic structure to the coordination number of the metal centre in this family of complexes, and possibly to the theoretical approach used. Interestingly, TD-DFT calculations on both triplet [Cr(dpqpy)(Cl)$_2$] and quintet [Cr(dpqpy)]$^{2+}$ revealed that only the first leads to multiple absorption bands in the 400-800 nm range in accordance with the experimental absorption spectrum recorded in DMF (**Figure S27-S29**). The most intense transitions are predicted at 647 and 495 nm for [Cr(dpqpy)(Cl)$_2$], and are attributed to intra-ligand charge transfers (**Figure S23**).

Further reduction yields the monoanion [Cr(dpqpy)(Cl)$_2$]$^-$, which could adopt doublet, quartet, or sextet spin states, all representing half-integer spin systems. The Mulliken spin population on the Cr centre is 2.89, 2.96 and 3.09, respectively, again arguing for mostly ligand-centred redox process, the last value comparing well with [Cr(dpqpy)(Cl)$_2$]$^+$ (**Table S5**). The doublet state is a broken symmetry (3,2) spin state, characterized by an antiferromagnetic interaction between a triplet diradical ligand (dpqpy$^{2•2-}$) and a Cr(III) metal ion (S = 3/2) (**Figure 6d**), and it is the ground state. This marked radical character is consistent with EPR spectroscopy, which reveals a low anisotropy of the g-tensor and a low spin state.

View Article Online
DOI: 10.1039/D6DT00748A

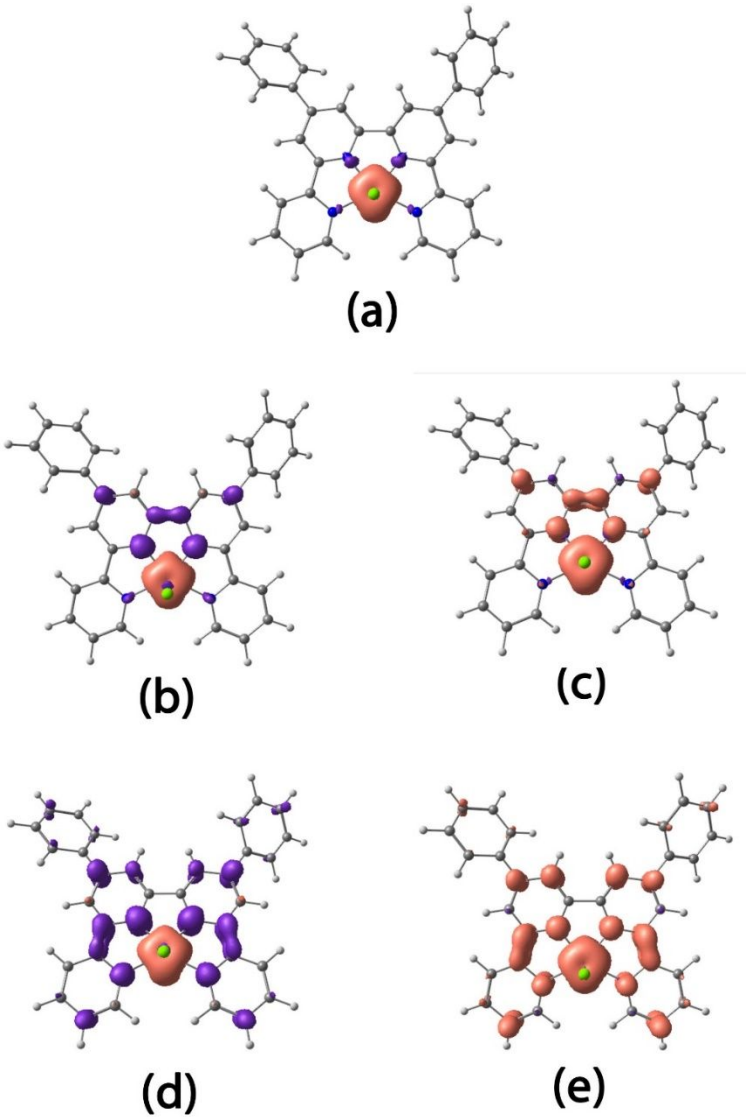

Figure 6. Spin density plot from a B3LYP/6-31g* calculation. Isosurface shown with 0.005410 contour value: a) $[Cr(dpqpy)(Cl)_2]^+$ (quartet); b) $[Cr(dpqpy)(Cl)_2]^0$ (broken symmetry triplet); c) $[Cr(dpqpy)(Cl)_2]^0$ (quintet); d) $[Cr(dpqpy)(Cl)_2]^{2-}$ (broken symmetry doublet); e) $[Cr(dpqpy)(Cl)_2]^{2-}$ (sextet).

The sextet state (+7.9 kcal/mol relative to the doublet, **Figure 6d**) results from ferromagnetic coupling, while the quartet lies intermediate, and is spin-contaminated due to its proximity with the sextet. Note that attempts to converge a Cr(III) complex featuring a closed-shell ($dpqpy^{2-}$) ligand, especially using the fragment approach, failed, highlighting the propensity of this ligand framework to support diradicals. This hypothesis is further supported by calculations on both the free ligand ($dpqpy^{2-}$) (**Figure S11**) and its Zn(II) complex (**Figure S12**), which point to a diradical ground spin state of the ligand, with geometrical specificities (tilt or umbrella-shape of the bipyridine core). This is also consistent with prior studies on terpyridine-based chromium

View Article Online
DOI: 10.1039/D6DT00748A

complexes by Wieghardt *et al.*, who demonstrated that the terpyridine dianion is stabilized under its diradical state (relative to the closed-shell state) by magnetic coupling.[37]

Table 1 Electronic structures and Mulliken spin populations of the Cr atom and the central N atoms in the dpqpy ligand for chromium complexes in their ground spin state [a]

Complex	Spin state	Mull. Spin pop. at Cr/N	Formulation	Metal ion geometry
$[Cr(dpqpy)(Cl)_2]^+$	Quartet	3.03/-0.05	Cr^{III}/ qpy	Octahedral
$[Cr(dpqpy)(Cl)_2]^0$	BS triplet	2.96/-0.22	Cr^{III}/ $qpy^{\bullet-}$	Octahedral
$[Cr(dpqpy)(Cl)_2]^-$	BS doublet	2.94/-0.27	Cr^{III}/ $qpy^{2\bullet2-}$	Octahedral
$[Cr(dpqpy)(Cl)]^0$, DMF	BS quartet	3.53/-0.18	Cr^{III}/ $qpy^{2\bullet2-}$ $\leftrightarrow Cr^{II}$/ $qpy^{\bullet-}$	Square pyramidal

[a] From a B3LYP/6-31g* calculation. The data for all the oxidation states and spin states, including the free energy differences between each spin states for a given complex, are detailed in ESI. (BS= broken symmetry).

It is worth noting that electrochemistry suggests that two-electron reduction of $[Cr^{III}(dpqpy)(Cl)_2]^+$ may be accompanied by the release of one chloride ion in solution. Thus, the electronic structure of the neutral species [Cr(dpqpy)(Cl)(DMF)] was also computed, again under the doublet, quartet and sextet spin states (**Table S2**). The doublet and quartet are close in energy (ΔE = 3.3 kcal/mol), the second being the most stable spin state, while the sextet is much higher in energy, 13.7 kcal/mol above the quartet. The doublet state is characterized by an octahedral Cr(III) centre, harbouring a Mulliken spin population of 2.83, with negative spin population on the coordination bipyridine nitrogens (-0.24 and -0.14). Thus, it is formulated as a $Cr^{III}(qpy^{2\bullet2-})$ radical species, similarly to the triplet $[Cr(dpqpy)(Cl)_2]^-$. The sextet is also better described as as $Cr^{III}(qpy^{2\bullet2-})$, although with ferromagnetic interactions. In contrast, in the quartet state, the Mulliken spin population is 3.67 on the Cr atom, e.g. between high spin Cr(II) and Cr(III), while the DMF ligand is released during the optimization, affording a square pyramidal metal centre (**Table S5**). This suggests that the energy gap between the $Cr^{III}(qpy^{2\bullet2-})$ and $Cr^{II}(qpy^{\bullet-})$ valence tautomers is reduced, due to the square pyramidal geometry and the less efficient metal charge compensation (due to the lack of one anionic ligand), both favouring a Cr(II) centre. This Cr(II) stabilization becomes even more pronounced when optimization is performed on a species lacking axial ligands ($[Cr(dpqpy)]^+$): the broken-symmetry quartet state is now formally a Cr(II) centre (Mulliken spin population of 3.94) coordinated to a ligand-based radical, and it is the ground state, lying just 0.5 kcal/mol above the sextet. Notably, TD-DFT

View Article Online
DOI: 10.1039/D6DT00748A

calculations consistently predict a rich visible absorption spectrum, irrespective of the nature of the axial ligand, and even in its absence (**Figures S27-S29)**. The assignment of the most intense bands is provided in ESI (**Figure S26**).

Electrocatalytic reduction of CO_2

Further electrochemical analyses of $[Cr(dpqpy)(Cl)_2]^+$ were carried out under a CO_2-saturated atmosphere to investigate its electrocatalytic properties. As shown in **Figure 7**, the CV scan under CO_2-saturated conditions resulted in a current increase at an onset potential of -1.77 V. This is accompanied to the loss of the reversibility behaviour of the third reduction waves as a more probable consequence of an inner-sphere mechanism for the catalysis

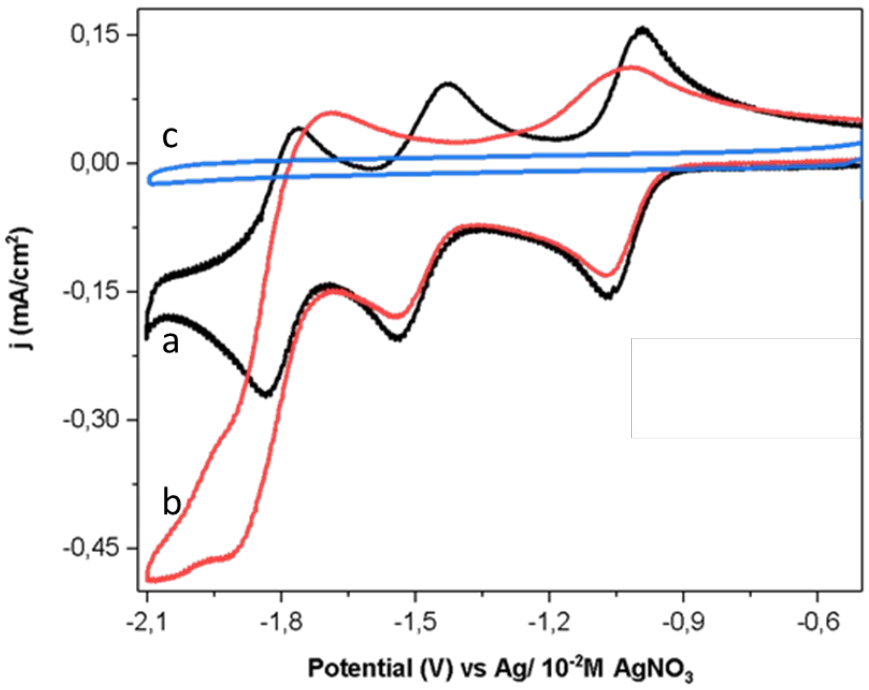

Figure 7 Cathodic scan cyclic voltammograms of $[Cr^{III}(dpqpy)(Cl)_2]^+$ under argon (a), CO_2 (b) and of a blank CO_2 saturated electrolyte solution (c) on GCE in DMF/0.1M $TBAPF_6$ at a scan rate of 0.1Vs^{-1} (electrode area 0.071 cm^2).

To improve the current response of the complex under CO_2, a weak acid, specifically phenol (PhOH), acting as a source of protons has been added in solution (**Figure 8)**.

View Article Online
DOI: 10.1039/D6DT00748A

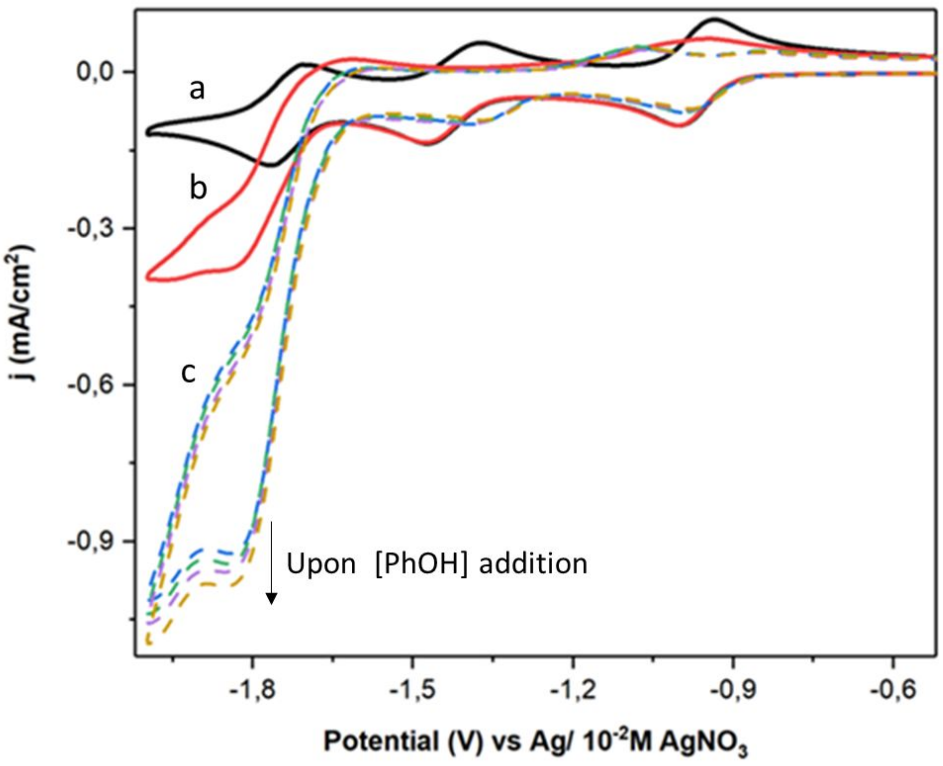

Figure 8. Cathodic cyclic voltammetry scans of a 1 mM $[Cr(dpqpy)(Cl)_2]^+$ complex under argon (a) and under CO_2 saturated condition without (b) and with varying concentration of [PhOH] (c) (1 M, 1.25 M, 1.5 M and 1.75 M) on GCE in DMF/0.1M $TBAPF_6$ at a scan rate of 0.1 Vs^{-1}.

A significant onset potential shift of ~50 mV was noted upon addition of 1 M of PhOH; the second reduction wave is also shifted to less negative potential and suggest that PhOH interact after the first reduction event of the complex. A further increase of the phenol concentration did not show a noticeable difference of the onset potential value; it mainly resulted in an increase of the catalytic peak current. The use of PhOH gave the best current response among that observed for other weak acids considered such as water or methanol in DMF (**Figure S30** and **S31** respectively).

Gas chromatography measurements, were performed to analyse the gas produced during four hours of exhaustive electrolysis of 1mM $[Cr(qpy)(Cl)_2]^+$ in the presence of different concentrations of phenol at a bias of -1.85 V. These analyses confirmed the formation of CO, with, in most case, no H_2 detected (cf. **Figure S32** as example of the chromatogram obtained). **Tables S7 -S10** gather the results obtained during the bulk electrolysis. A small amount of H_2 is only observed when using a concentration of PhOH of 1.75 M and after 2hrs of electrolysis (**Table 2**). **Figure 9** shows the evolution of CO production throughout the 4h electrolysis

View Article Online
DOI: 10.1039/D6DT00748A

measurements with different concentrations of PhOH in solution. In all case, the production of CO increased during the first two hours and then stabilized for the rest of the remaining time. Concomitantly, we noticed in all case a decrease in the magnitude of the cathodic catalytic current after 2hrs (**Figure S33**). It suggests a degradation of the complex or a poisoning of the electrode surface, rather than the consumption of CO towards more elaborated products. Electrolysis in the presence of 1.25 M PhOH resulted in a higher amount of produced CO among all varied concentrations, yielding a 60 % ± 10 % faradaic efficiency after two hours (**Table 2).** After the 4h electrolysis no formation of $HCOO^-$ in solution was detected by ionic chromatography

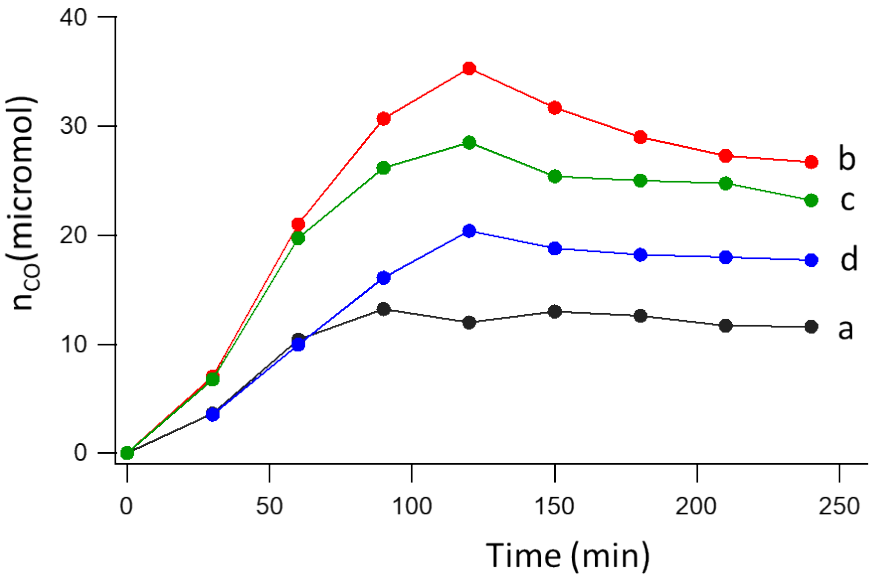

Figure 9. Evolution of the amount of CO produced during electrolysis of 1mM $[Cr(qpy)(Cl)_2]^+$ complex at -1.85V Ag/10^{-2}M $AgNO_3$ under CO_2-saturated conditions with varying concentration of PhOH (a : 1M, b: 1.25 M, c: 1.5 M, d: 1.75 M) on a carbon foam electrode in DMF/0,1M $TBAPF_6$.

.

Table 2. Faradaic efficiency (F.E.) for the production of CO and H_2 during the electrochemical CO_2 reduction with 1 mM $[Cr(qpy)(Cl)_2]^+$ complex as catalyst in the presence of a varying concentration of phenol (PhOH) after a 2h electrolysis at -1.85 V *vs* $Ag/AgNO_3$ on a carbon foam electrode in CO_2-saturated DMF/0,1M $TBAPF_6$. Uncertainties are estimated to ±10%.

[PhOH]	Q (C)	F.E. CO (%)	F.E. H_2 (%)
1 M	-12.8	18	-
1.25 M	- 11.4	60	-
1.5 M	- 10.3	55	-
1.75 M	-11.2	35	1

View Article Online
DOI: 10.1039/D6DT00748A

The foot of the wave analysis (FOWA),[38,39] following equations 2-4, was performed on cyclic voltammograms of a 1 mM solution of $[Cr(dpqpy)(Cl)_2]^+$ in DMF containing 0.1 M $TBAPF_6$, under CO_2-saturated conditions, both in the absence and presence of 1.25 M PhOH. This analysis was used to estimate the catalytic rate constant (k_{obs}), as well as the turnover frequency (TOF) and turnover number (TON) after 2 hours under both conditions, without and with addition of PhOH.

$$\frac{i}{i_p^0} = \frac{2{,}24\sqrt{\frac{RT\ 2k_{obs.}}{Fv}}}{1 + exp\left[\frac{F}{RT}(E - E^0)\right]} \qquad (eq.2)$$

$$TOF = \frac{k_{obs}}{1 + exp\left[\frac{F}{RT}(E - E^0)\right]} \qquad (eq.3)$$

$$TON = TOF \times t \qquad (eq.4)$$

In these equations, *v* is the scan rate, E° = -1.79 V, i and i_p^0 the peak current under catalytic condition and under argon respectively.

The FOWA plots (**Figure S34**) yield k_{obs} values of 0.62 s^{-1} and 8.74 s^{-1} in the absence and presence of PhOH (1.25 M), respectively, indicating a 14-fold increase in the reaction rate upon addition of the proton source. The TOF at E = −1.85 V is estimated to be 0.56 s^{-1} without PhOH and 8 s^{-1} with PhOH. In the presence of PhOH, the TOF is comparable to values reported for other Cr(III)-based catalysts;[18,40] however, it remains approximately one order of magnitude lower than that obtained for $[Cr(qpy)(Cl)_2]^+$, indicating that diphenyl substitution has a detrimental effect on catalytic performance. After 2 hours, the maximum TON is estimated to be 5.7×10^4, significantly lower than the value of 1.56×10^5 reported for $[Cr(qpy)(Cl)_2]^+$, suggesting reduced catalyst stability.

Conclusion:

In the present work the synthesis and reactivity of a diphenyl quaterpyridine Cr(III) complex that displayed substantial catalytic activity towards CO_2 reduction has been described. The

View Article Online
DOI: 10.1039/D6DT00748A

catalysis occurs after a three-reductions process of the complex. Its efficiency is improved in presence of 1.25 M phenol as proton source in DMF, reaching a maximum of 60 % ± 10% faradaic efficiency for the formation CO after 2 hrs. The complex undergoes degradation after 2 hours of electrolysis, resulting to a cessation of the catalytic activity. It confirms however the interest of Cr(III) based complexes to design new molecular catalysts. Characterization of the complex under argon by electrochemistry and EPR supported by DFT calculation shows that the first reduction event of the complex is more probably centred on the metal, whereas the second and third reduction are localized on the ligand, highlighting the propensity of this ligand framework to support diradicals. This suggest at least an appropriate degree of electronic coupling between the metal centre and the redox active ligand to allow for an efficient reactivity under CO_2.[41,42] Indeed, the electron storage ability of the ligand associated to an open coordination site on the metal is required for the two-electron two-proton CO_2 reduction process. Further work needs to be carried on in order to deeply investigate the catalytic cycle and then to improve the long-term stability of such complex upon catalysis. One way to improve stability is to anchor the complex onto the electrode surface, either by forming a polymer or by creating a self-assembled monolayer following specific modifications on the quaterpyridine ligand. Conversely, the use of less sterically hindered quaterpyridines appears to enhance catalytic performance, particularly in terms of faradaic efficiency and TOF.

Acknowledgement: The authors thank the ANR project solar driven chemistry (ANR-20-SODR-0001-01) and Labex Arcane (ANR-17-EURE-0003) for financial support, and the referees for their comments to improve the quality of the work. J.C. thanks Alain Deronzier for fruitful discussions. Part of the work have been performed using the ICMG characterization platform and mass spectrum facilities from Université Grenoble Alpes.

Bibliography:

1. R. Francke, B. Schille, M. Roemelt, *Chem. Rev.*, **2018**, *118*, 4631-4701.
2. D. D. Zu, J. L. Liu, S. Z. Qiao, *Adv. Mater.*, **2016**, *28*, 3423–3452.
3. A. M. Appel, J.E. Bercaw, A. B. Bocarsly, H. Dobbek, D. L. DuBois, M. Dupuis, J. G. Ferry, E. Fujita, R. Hille, P. J. A. Kenis, C. A. Kerfeld, R. H. Morris, C. H. F. Peden, A.

R. Portis, S. W. Ragsdale, T. B. Rauchfuss, J. N. H. Reek, L. C. Seefeldt, R. K. Thauer, G. L. Waldrop, *Chem. Rev*., **2013**, *113* (8), 6621–6658.

4. B. Kumar, M. Llorente, J. Froehlich, T. Dang, A. Sathrum, C. P. Kubiak, *Annu. Rev. Phys. Chem*., **2012**, *63*, 541-569.
5. J. Hawecker, J. M. Lehn, R. Ziessel, *Helv. Chim. Acta*, **1986**, *69*, 1990-2012.
6. H. Ishida, K. Tanaka, T. Tanaka, *Organometallics*, **1987**, *6*, 181-186.
7. C. M. Bolinger, N. Story, B. P. Sullivan, T. J. Meyer, *Inorg. Chem*., **1988**, *27*, 4582-4587.
8. M. Stanbury, J.-D. Compain S. Chardon-Noblat, *Coord. Chem. Rev.,* **2018**, *361*, 120−137.
9. K. E. Dalle, J. Warnan, J. J. Leung, B. Reuillard, I. S. Karmel, E. Reisner, *Chem. Rev.,* **2019**, *119*, 2752−2875.
10. J.-W. Wang, W.-J. Liu, D.-C. Zhong, T.-B. Lu, *Coord. Chem. Rev.,* **2019**, *378*, 237-261.
11. E. A. Palade, R. Gobetto, C. Nervi, *Inorg. Chim. Acta,* **2024***, 566*, 122029.
12. K. A. Grice, *Coord. Chem. Rev*., **2017**, *336*, 78-95.
13. M. E. Moberg, C. W. Machan, *Acc. Chem. Res.* **2024**, *57*, 2326-2335
14. J. Tory, B. Setterfield-Price, R. A. W. Dryfe, F. Hartl, *ChemElectroChem.*, **2015**, *2*, 213–217.
15. J. A. Ramos Sende, C. R. Arana, L. Hernandez, K. T. Potts, M. Keshevarz-K, H. D. Abruña, *Inorg. Chem*., **1995**, *34* (12), 3339–3348.
16. S. L. Hooe, J. M. Dressel, D. A. Dickie, C. W. Machan, *ACS Catal*., **2020**, *10*(2), 1146-1151.
17. A. G. Reid, S. L. Hooe, J. J. Moreno, D. D. Dickie, C. W. Machan, *Inorg. Chem.*, **2022**, *61*, 16963-16970.
18. J.-W. Wang, Z.-M. Luo, G. Yang, M. Gil-Sepulcre, S. Kupfer, O. Rudiger, G. Ouyang, PNAS, **2024**, *121*(14), e2319288121
19. K.-M. Lam, K.-Y. Wong, S.-M. Yang, C.-M. Che, *J. Chem. Soc., Dalton Trans.,* **1995**, 1103−1107.
20. Z. Guo, F. YU, Y.Yang, C.F. Leung, S.-M. Ng, C.-C. Ko, C. Cometto, T.-C. Lau, M. Robert, *ChemSusChem*, **2017**, *10*, 4009-4013.
21. C. Cometto, L. Chen, P. K. Lo, Z. Guo, K.-C. Lau, E. Anxolabéhère-Mallart, C. Fave, T.-C. Lau, R. Robert, *ACS Catal*., **2018**, *8*, 3411-3417.

22. L. Chen, G. Chen, C.-F. Leung, C. Cometto, M. Robert, T.-C. Lau, *Chem. Soc. Rev.*, **2020**, *49*, 7271-7283
23. E. C. Constable, S. M. Elder, D. A. Tocher, *Polyhedron*., **1992,** *11*, 1337-1342.
24. E. C. Constable, M. J. Hannon, P. Harverson, M. Neuburger, D. R. Smith, V. F. Wanner, L. A. Whall, M. Zehnder, *Polyhedron*., **2000**, *19*, 23-34.
25. V. V. Pavlishchuk, A. W. Addison, *Inorg. Chim. Acta*, **2000**, *298*, 97-102.
26. M. J. Frisch et al., *Gaussian 09, Revision D.01*, Gaussian, Inc., Wallingford CT, 2009.
27. C. Lee, W. Yang and R. G. Parr, *Phys. Rev. B: Condens. Matter Mater. Phys.*, **1988**, *37*, 785-789.
28. A. D. Becke, *J. Chem. Phys.*, **1993**, *98*, 5648-5652.
29. S. Grimme, J. Antony, S. Ehrlich, H. Krieg, *J. Chem. Phys*., **2010**, *132*, 154104G.
30. A. Petersson, M. A. Al-Laham, *J. Chem. Phys.*, **1991**, *94*, 6081-6090.
31. A. D. McLean, G. S. Chandler, *J. Chem. Phys.*, **1980**, *72*, 5639-48.
32. K. Raghavachari, J. S. Binkley, R. Seeger, J. A. Pople, *J. Chem. Phys*., **1980**, 72, 650-54.
33. J. Tomasi, B. Mennucci, R. Cammi, *Chem. Rev*., **2005**, 105, 2999-3093.
34. G. Cauquis, A. Deronzier, B. Sillion, B ; Damin, J. Garapon, *J. Electroanal. Chem.*, **1981**, *117*, 139-146.
35. R. Farran, L. Le-Quang, J.-M. Mouesca, V. Maurel, D. Jouvenot, F. Loiseau, A. Deronzier, J. Chauvin, *Dalton Trans.*, **2019**, *48*, 6800-6811.
36. R. P. Bonomo, A. J. Di Bilio, F. Riggi, *Chem. Phys.*, **1991**, *151*, 323-333
37. C. C. Scarborough, K. M. Lancaster, S. DeBeer, T. Weyhermüller, S. Sproules, K. Wieghardt; *Inorg. Chem*., **2012**, *51* (6), 3718-3732.
38. C. Costentin, S. Drouet, G. Passard, M. Robert, J.-M. Savéant, *J. Am. Chem. Soc*., **2013**, *135*, 9023-9031.
39. C. Costentin, J.-M. Savéant, *ChemElectroChem*, **2014**, *1*, 1226-1236.
40. M.E. Moberg, A. G. Reid, D. A. Dickie, C. W. Machan, Dalton Trans., 2024, 53, 16849-16860.
41. C. R. Hess, T. Weyhermüller, E. Bill, K. Wieghardt, *Inorg. Chem*., **2010**, *49*, 5686-5700
42. J. J. Moreno, S. L. Hooe, C. W. Machan, *Inorg. Chem*. **2021**, *60*, 3635−3650.

View Article Online
DOI: 10.1039/D6DT00748A

Article ref. DT-ART-04-2026-000748,

Title : Synthesis, characterisation and properties towards CO_2 reduction into CO of a Cr(III) diphenyl quaterpyridine complex.

Authors : Kabibi-Charles Kamashanju, Mathieu Curtil, Florian Molton, Nikolaos Vlachopoulos, Fabrice Thomas, Jérôme Chauvin

Data availabilities :

The data supporting this article have been included as part of the supplementary information.

Sincerely,

Jérôme Chauvin (corresponding author)